IEEE Journal of Microwaves

Received 26 May 2023; revised 21 August 2023; accepted 25 August 2023. Date of publication 15 September 2023; date of current version 9 October 2023.

Digital Object Identifier 10.1109/JMW.2023.3310889

Beam Steerable Half Mode SIW Leaky-Wave Antenna Using FPMS

SHAHINSHAH ALI [1] (Student Member, IEEE), HAMMAD M. CHEEMA [2] (Senior Member, IEEE), AND FARHAN A. GHAFFAR [1] (Senior Member, IEEE)

(Regular Paper)

[1]Department of Electrical Engineering, Lakehead University, Thunder Bay, ON P7B 5E1, Canada
[2]Research Institute for Microwave and Millimeter-wave Studies, National University of Sciences and Technology, Islamabad 44000, Pakistan

CORRESPONDING AUTHOR: Farhan A. Ghaffar (e-mail: fghaffar@lakeheadu.ca).

This work was supported by NSERC Discovery Grant RGPIN-2020-05614.

ABSTRACT A novel leaky wave antenna (LWA) with integrated field-programmable microwave substrate (FPMS) unit cells is presented in this article. The proposed antenna consists of a Half Mode Substrate Waveguide (HMSIW), loaded with cross-shaped slots to generate the desired phase response and radiation characteristics. Using the agile FPMS technology, the substrate properties along one of the longitudinal edges of the antenna are varied, which allows the steering of the radiation direction at a single frequency. A total of 70-unit cells are integrated with the antenna at 12 GHz, resulting in a maximum beam steering of 72° in simulations along the elevation. Experimental results of the fabricated prototype also demonstrate the practical viability of the proposed design concept with a total beam steering of 35°. The design presented in this research serves as a proof-of-concept, setting the stage for forthcoming advancements and refinements in the field of smart antenna systems using FPMS.

INDEX TERMS Field programmable microwave substrate (FPMS), leaky wave antenna (LWA), half mode substrate waveguide (HMSIW).

I. INTRODUCTION

Antennas with directive beam patterns are popular for their use in applications such as radar, satellites, and, more recently, 5G and the Internet of things (IoT) communication. The inclusion of beam steering capabilities into directional antennas enhances their usage in modern wireless applications that rely greatly on smart radio frequency (RF) components. Among the various antenna choices suitable for these applications, leaky wave antennas (LWAs) provide a simple mechanism to obtain highly directive and steerable radiation performance [1]. In addition, this class of antenna has a low profile and simple fabrication, which are desirable traits in today's electronics [2]. These characteristics allow their seamless integration into microwave and millimeter wave applications such as automotive radar, surveillance, and other military and commercial applications [3].

A variety of LWA designs have been reported in the literature that demonstrate antenna beam steering by changing the frequency of the input RF wave [4], [5], [6], [7], [8]. Using this classical method, the phase constant and wave number of the propagating wave are altered, resulting in the maximum of the radiation to steer. However, most modern wireless communication systems operate at a fixed center frequency with some bandwidth allocated to them [9]. This dispersive nature of LWAs makes them unfit to be employed in wireless applications unless the beam scanning can be achieved at a single frequency.

To circumvent this problem, in recent publications, different structures have been proposed to design LWAs where the beam can be steered at a single center frequency. A popular technique among these proposals is integrating active components, such as PIN [10] and varactor diodes [11], onto the antenna structure. By modulating the switching states of these diodes, the effective width of the waveguide is controlled, thus enabling a dynamic change in the propagation constant of the wave and the direction of maximum radiation. Likewise, in [12], a half-width microstrip LWA is proposed that can steer the antenna's main beam at a fixed frequency with the

help of capacitor loading. These capacitors are analogous to the diodes used in the previous two examples, and therefore it can be said that the design relies on the same operating mechanism. Employing the concept of varactor integration, the authors in [13] modulated the surface impedance of the propagating wave. Using a triangular profile for impedance modulation, the design demonstrates beam steering at a fixed antenna frequency. A significant endeavor has been undertaken to design substrate integrated waveguide (SIW) based composite right-/left-handed (CRLH) LWAs, with the aim of enabling continuous scanning of the beam from backward to forward direction while passing through the broadside radiation [14], [15]. From this brief summary of literature, it can be deduced that some work done in the area of single frequency-based LWA designs has been reported previously; however, the research in this domain can be further flourished by using newer technologies. For this purpose, a new FPMS-based LWA design is proposed in this work. The concept of FPMS and its use in RF circuits recently evolved from a research group at Carleton University [16]. Reconfigurable high-frequency circuits, such as filters, amplifiers, and oscillators, have been reported since then as a steppingstone for this technology [16], [17]. The level of programmability that this technology can bring to the RF circuits can result in a paradigm shift in the design of smart reconfigurable wireless components. However, the use of this technology is on the leaner side when it comes to antennas [18], [19]. An HMSIW-based antenna that can steer the beam only in the forward direction is the best demonstration of FPMS in antenna domain up to-date [20]. However, this article is not able to show continuous steering from backward to forward direction with the measured results of 25°. The other concern is the lack of FPMS unit cell characterization. This is a major downside. The absence of the unit cell study in [20] results in a partial understanding of the technology for the readers. Finally, the antenna loses its optimum matching state, when the unit cells are biased to achieve maximum steering thus reducing the antenna gain. Considering these limitations, this study addresses the downsides of the reported antenna element. At first, a complete study of the FPMS unit cells at a much higher frequency (12 GHz) has been introduced for the first time. This study forms the basis of the proposed antenna structure shown in Fig. 1. The antenna is designed to show optimum matching conditions while steering the main beam from backward to forward direction. Notably, the approach ensures the absence of an open stop band gap at the operating frequency providing a stable broadside radiation. The antenna prototype provides a maximum measured gain of 6.2 dBi with a steering range of 35°, hence providing a proof-of-concept for using the FPMS technology for the design of adaptable RF components.

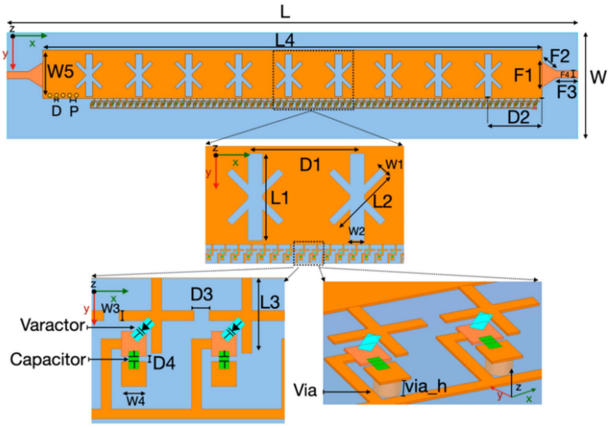

FIGURE 1. Schematic design of HMSIW LWA.

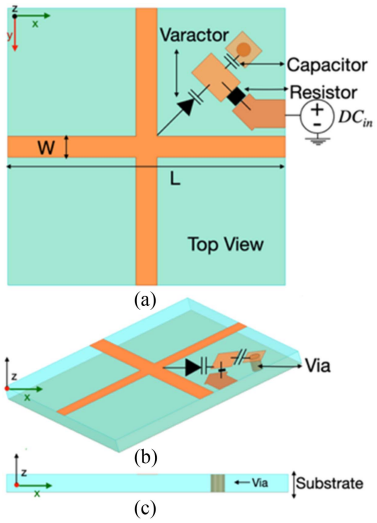

FIGURE 2. Schematic design of FPMS. Varactor: *sky-works SMV1430.* (a) Top view of FPMS unit cell (L_{FPMS} = 1.5 mm and W_{FPMS} = 0.2 mm) (b) incline view of FPMS unit cell (c) side view of FPMS unit cell.

II. ANALYSIS OF FPMS UNIT CELL

The fundamental building block of FPMS technology is a unit cell structure shown in Fig. 2. This structure consists of two microstrip lines connected normally to each other, thus forming a cross-patch. A varactor diode is integrated at the point of intersection of the two lines that can be biased to change the capacitance value loaded onto the structure. The anode of the varactor is directly connected to the cross-patch, and the DC voltage is applied to the cathode of the varactor via the 10 kΩ resistor. The purpose of the resistor is to isolate the DC bias from the RF signal and thus acts as an RF choke. A DC-block capacitor of 10 pF provides the path for the high-frequency signal to pass through the varactor into the ground. By varying the applied bias on the varactor, the impedance of the unit cell experienced by the incoming RF wave can be controlled. Using Nicolson-Ross-Weir (NRW) algorithms [21] in tandem with the basics of Transmission Line Theory, the effective substrate properties, particularly the dielectric properties, can be determined for a range of frequencies. For this purpose, the S-parameters of the FPMS unit cell are studied with the varying capacitance values of the varactor diode. These S-parameters are used as an input to the

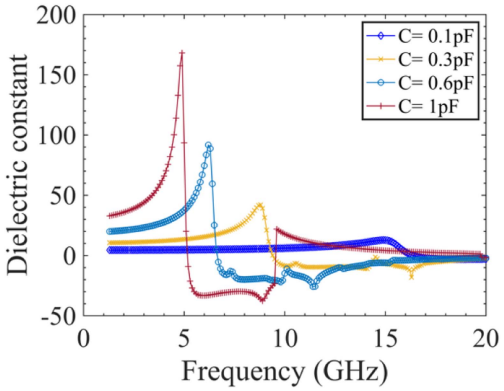

FIGURE 3. Dielectric constant of roger RT5870 substrate at different DC voltages applied through varactor.

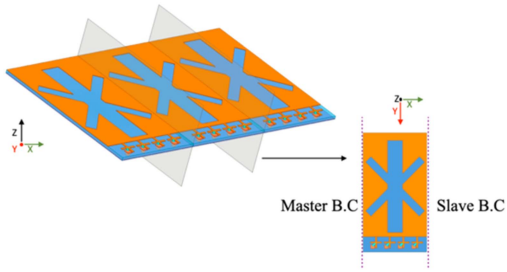

FIGURE 4. Radiating unit cell with FPMS for dispersion analysis.

NRW algorithm, which, in turn, provides the resulting substrate characteristics for varying varactor bias. A predictable range of permittivity can be achieved by carefully adjusting the size of the unit cell and choosing the right range of the varactor diode.

Although this part of the FPMS unit cell design has been discussed in [16], the limitation in that case, is the upper-frequency limit. The characterization shown in [16] is only up to 4 GHz, which makes it unsuitable to be directly employed in this work. Therefore, a fresh study of the unit cell at higher frequencies is needed as the first step. Keeping X-band as the target range for the antenna design, the dimensions of the unit cell are varied while keeping a close eye on the frequency response of the structure. Initially, the size of the cell is reduced from 5.08 mm [16] in order to increase the resonant frequency of the structure. Using Duroid 5870 as the substrate, the structure is simulated in the full-wave simulator Ansys HFSS. Duroid 5870 is selected for this work because of its low loss tangent ($tan\delta$) value, making it an excellent candidate for antenna design. Although HFSS does not need a specific varactor model for antenna simulation, it is important to ascertain the one to be used in this design. This will help define the range of the capacitance to be used in the simulations along with its equivalent lumped circuit model. SMV1430 is chosen as a suitable candidate because of its tunable range and frequency. The capacitance of the varactor is varied from 0.1 pF to 1.0 pF while plotting the S-parameters of the unit cells. Using these simulations, the dielectric constant experienced by the propagating RF wave is plotted in Fig. 3.

The range of positive values of permittivity depends on the range of capacitance that is used in these simulations (Fig. 3). The results show that for a given value of capacitance, the wave experiences a positive dielectric constant until the structure starts to resonate. Thereafter, the evanescence of waves can be observed due to the negative permittivity values. It means that beyond the resonant frequency, the overall reactance of the unit cell shows an inductive effect. This characteristic of the FPMS unit cell is especially useful in LWA design as it provides the designer with the control of the substrate properties. With the range of capacitance mentioned above, the dielectric constant of the unit cell is seen to change from 5 to 30 at low frequencies (∼1 GHz). Furthermore, it is observed that the increase in the capacitance of the varactor has a direct effect on the resonant frequency. For instance, the resonant frequency decreases from 15 GHz to 5 GHz as the capacitance increases from 0.1 pF to 1.0 pF. At the design frequency of 12 GHz, the dielectric constant starts from positive values for a lower varactor bias and then switches to negative ones as the bias is increased. Both positive and negative dielectric constants are useful for LWA design as the wave propagation can be controlled by employing either one of them. This will be further explained in the sections to follow. From this study, the optimal length and width of the lines used in the unit cell design are selected to be 1.5 mm and 0.2 mm, respectively, while the capacitance range is determined to be 0.1 pF to 1.0 pF. It should be noted here, that the range of the varactor bias used here is still preliminary since the integration of the unit cells onto the antenna may require further optimization.

III. DISPERSION DIAGRAM OF A UNIT LWA STRUCTURE

The complete LWA design that relies on an HMSIW structure is shown in Fig. 1. Cross-shaped slots are etched together with the transverse slots on the top layer, while the bottom metallic layer is a solid ground plane. These slots allow the leaking of the wave along the length of the antenna by providing the required variation in the wave impedance. To make the antenna steerable at a single frequency, FPMS unit cells are integrated along the length of the antenna on one of its edges. Before delving into the study of the antenna's impedance and radiation performance, it is useful to study the propagation constant of the wave on the leaky wave structure of Fig. 1. For this purpose, radiating unit cell of Fig. 4 is simulated in the eigenmode of Ansys HFSS to study the phase constant, β and attenuation constant, α of the propagating RF wave. The S-parameters obtained from these simulations are used as the input to the Transmission Line equations presented in [22]:

$$\beta = \frac{1}{p}\left|\mathbf{Im}\left(\cosh^{-1}\left(\frac{1-S_{11}S_{22}+S_{12}S_{21}}{2S_{21}}\right)\right)\right| \quad (1a)$$

$$\alpha = \frac{1}{p}\left|\mathbf{Re}\left(\cosh^{-1}\left(\frac{1-S_{11}S_{22}+S_{12}S_{21}}{2S_{21}}\right)\right)\right| \quad (1b)$$

TABLE 1 Dimensions of LWA

Length (mm)		Distance (mm)		Width (mm)		Microstrip feed line (mm)		Via (mm)	
L	160.15	D	0.2	W1	1	F1	6.99	p	0.8
L1	12	D1	14	W2	2	F2	4.7	Via_h	.254
L2	10	D2	9	W3	0.2	F3	6		
L3	1.5	D3	0.3	W4	0.4	F4	2		
L4	140.15	D4	0.1	W5	13.55				

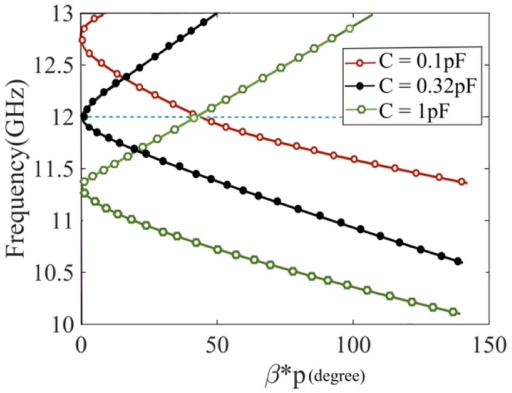

FIGURE 5. Dispersion plot of radiating elements shown in Fig. 4 with integrated FPMS cells.

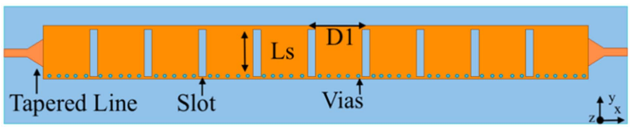

FIGURE 6. Schematic design of LWA with transverse slots (dimensions provided in Table 1).

where p is distance between radiating unit cells.

The dimensions used in these simulations are the same as the final antenna design and are included in Table 1. The analysis of the propagation constant, γ of the wave on the radiating structure of Fig. 4 is important to understand the mode of operation and how the wave leaks from it as it propagates longitudinally on the structure. For this purpose, the dispersion graph of the radiating unit cell is simulated with three different values of capacitance, shown in Fig. 5. To illustrate the concept, two values of capacitance ($C = 0.1$ pF and $C = 1$ pF) are chosen, representing the extreme cases of steering, while the intermediate value of capacitance ($C = 0.32$ pF) shows the steering in the broadside direction. It can be observed that when the unit cell is simulated with a 0.1 pF capacitance, the antenna radiates in the backward direction at 12 GHz, whereas for the other extreme, i.e., 1 pF the radiation shifts to the forward direction. Furthermore, the dispersion curve does not exhibit an open stop band gap. Consequently, the antenna can radiate in the broadside direction without any degradation in the gain (for $C = 0.32$ pF). Also, the same graph illustrates the frequency shift in the dispersion curve as the value of C is increased. Thereby showing a shift from 12.75 GHz to 11.45 GHz while moving from one extreme to the other. The plot also demonstrates the natural operation of leaky-wave antenna where one can steer the antenna beam by changing the frequency of the input signal at a single capacitance value. However, using FPMS, this steering can be achieved by varying the bias on the varactor diode (changing the capacitance value), thus causing the phase constant (β) to vary at a particular frequency. The authors wish to exploit this property of FPMS in the subsequent section of this article and see its effect on antenna radiation. Moreover, these simulations show that below 13.5 GHz, the normalized phase constant ($\frac{\beta}{k_0}$) of the leaky mode is less than 1, which indicates that the mode is a fast wave with a solution in the physical region (where k_0 is the free space wavenumber). Within the same frequency range, the normalized attenuation constant, α, is almost zero, indicating minimum loss due to the dielectric properties of the substrate. This propagating mode is known as the surface-wave mode. As the frequency of the incoming wave increases, the surface mode starts to dominate the propagation, causing a reduction in the leaky mode. Furthermore, as the frequency approaches the leaky-mode cutoff (13.5 GHz), the mode rapidly loses physical significance, resulting in a very small percentage of the leaky mode. When the frequency exceeds 13.5 GHz, the phase constant of the leaky mode becomes greater than k_0, indicating that the mode has transformed into a slow wave with no physical significance. This is the fundamental theory that explains the propagation of leaky mode in the proposed antenna structure.

IV. ANTENNA DESIGN FOR CONTINOUS BEAM STEERING

Using the analysis of the previous two sections, the proposed antenna design is studied in this section for its impedance and radiation performance. At first, radiation performance of the transverse slot antenna, shown in Fig. 6, is analyzed using a full-wave simulator which extends into the cross-shaped slot

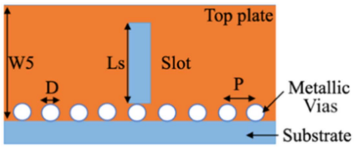

FIGURE 7. Schematic design of transverse slot unit cell.

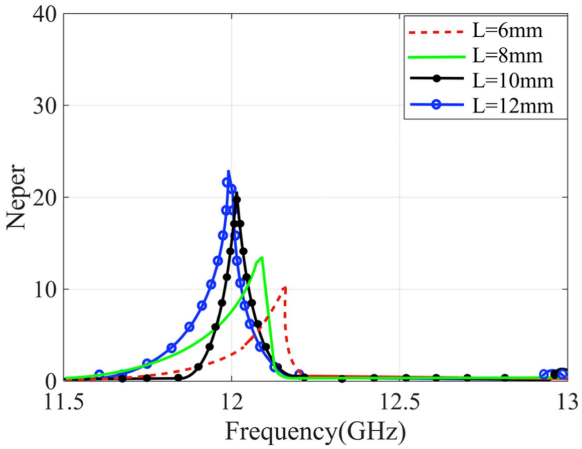

FIGURE 8. Leakage factor ($|\alpha.p|$) of Transverse slot unit cell.

SIW design of Fig. 1 that is eventually integrated with the FPMS unit cells.

A. TRANSVERSE SLOT LWA

To understand the radiation from the cross-shaped slots, it is pertinent to analyze the simple transverse slot waveguide of Fig. 6 for its radiation characteristics as it forms the basis of the final antenna structure [23]. For this purpose, a single slot is simulated in a short 28 mm waveguide structure of Fig. 7 to compare it with the unit cell of Fig. 4. Using a 0.254 mm thick RT5780 substrate, the design is optimized to operate at 12 GHz with the PEC wall realized using conventional metallic vias instead of FPMS unit cells. The operating frequency of the antenna helps to determine the width ($W5$) of the SIW structure. This gives the designer some latitude on the slot length ($\boldsymbol{L_s}$) while studying the wave propagation. By varying this value, the strength of the radiated wave can be maximized. The length is varied from 6 mm to 12 mm while paying attention to the radiation efficiency from the longitudinal slot. It is observed from these simulations that the efficiency of the radiating structure (Fig. 7) increases from 39% to 48% as the value of $\boldsymbol{L_s}$ is varied. The leakage factor measured in Neper, recorded from these simulations, is plotted in Fig. 8. The results correspond well with the theory, according to which the amount of energy escaping from such a slot maximizes once the slot reaches resonant length ($\sim\lambda_g$). For this design, λ_g comes out to be close to 16 mm; however, due to the waveguide width being ~14 mm, the slot length is kept at a maximum of 12 mm. This allows around 1 mm of clearance

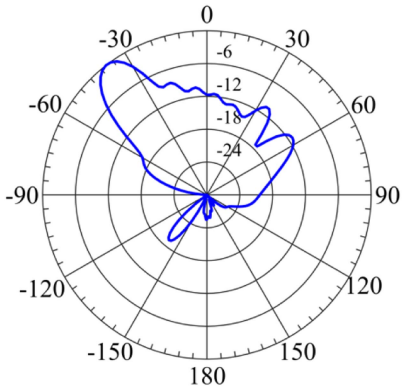

FIGURE 9. Normalized radiation pattern of LWA at 12 GHz without FPMS unit cells.

across the slot and can be deemed as practically realizable. Using the radiation analysis of the slot structure shown in Fig. 7, the transverse slot LWA design of Fig. 6 can now be studied for its capabilities as an antenna. The structure is fed with a tapered microstrip feed line that acts as an impedance converter between the 50-Ω feed and the input of the waveguide. The dimensions of the 50-Ω microstrip feed are calculated using the well-known microstrip line equations, while the dimensions of the tapered feed structure are optimized with the help of Ansys HFSS simulations. The same feed structure is kept consistent throughout the study of LWA design in this work. To ensure the leakage for the broadside beam, initially, 9 transverse slots are edged on the top plate of the half-mode waveguide. A series of metallic vias is integrated on one side of the waveguide, while the other side is left open-circuited to provide the PMC boundary condition. A maximum gain of 4 dBi is achieved in these simulations at an angle of $-45°$ from the elevation. The length of the antenna is kept the same as the one shown in Fig. 1 and listed in Table 1 i.e., $L4 = 140$ mm. By varying the distance between the slots and the length of the individual slots, the gain is optimized for its best value. However, it is deduced that 4 dBi is the maximum gain that can be extracted from the LWA design with simple transverse slots. The low gain value from this design is expected due to the limited leakage factor from the transverse slots (Fig. 8). Thus, to increase the gain further, the authors turned to the cross-shaped slot HMSIW LWA of Fig. 1, proposed in [23].

B. TRANSVERSE AND CROSS-SHAPED SLOT LWA

Subsequently, after studying the simple transverse slot antenna, the modified slots that rely on transverse and cross-shaped slots are introduced onto the waveguide, as shown in Fig. 1. Initially, the lateral edge of the waveguide consisted of simple metallic vias rather than the FPMS unit cells to realize the PEC boundary condition. The antenna design variables are tuned interactively while its performance is monitored. The focus of attention is on the antenna's radiation pattern while running these parametric simulations. The optimized normalized radiation of the antenna design is shown in Fig. 9

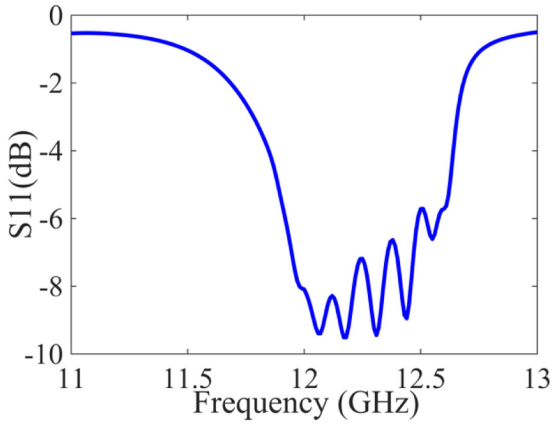

FIGURE 10. Reflection coefficient of LWA without FPMS unit cells.

with its final design parameters tabulated in Table 1. Like the conventional 1-D LWA; the antenna produces a fan-shaped beam, where the beam width is wider in the yz plane (H-plane) and narrower in the xz plane (E-plane). The antenna's gain is around 7.5 dBi with an acceptable reflection coefficient performance of – 10 dB at 12 GHz, Fig. 10. These results provide a good enough starting point where the FPMS unit cells can be integrated onto the SIW antenna.

The FPMS unit cells are integrated onto the antenna for capacitive loading. This is done while closely examining the antenna's radiation characteristics. To improve the input matching (S_{11}) performance, the starting edge of the LWA structure is kept unchanged by using metallic vias while 70 FPMS unit cells are integrated after leaving a length of ∼10 mm from the feeding edge. This modification makes the design non-symmetric and therefore it can only be fed from port 1 for the optimum performance of impedance and radiation. A future step could be to study the design as a symmetric structure with equal length of the antenna on both sides consisting of metallic vias. This will allow characterization and use of the antenna from either port/edge. It is also noted that the diameter of the vias and spacing between them (the ones used at the starting edge of port 1) changes the input impedance of the antenna, which after optimization are chosen to be 0.2 mm and 0.8 mm, respectively. The simulated radiation patterns of the LWA with varying capacitance of the varactor diode are shown in Fig. 11. The antenna main beam (in the xz-plane) steers from −35° to 37° as the capacitance of the varactor is altered from 0.1 pF to 0.6 pF. The radiation in the yz-plane (Fig. 11(b)) largely remains unaltered for different bias conditions, which is expected. The maximum gain of the antenna is 6.4 dBi for a capacitance value of 0.3 pF at 12 GHz. The gain value has slightly reduced due to the integration of FPMS unit cells. This is not surprising as these cells include lumped components (like the RF choke resistor) that will cause some dissipation of power and reduce antenna gain. As the capacitance of the varactor is altered, the gain of the antenna goes through a maximum variation of 2 dB.

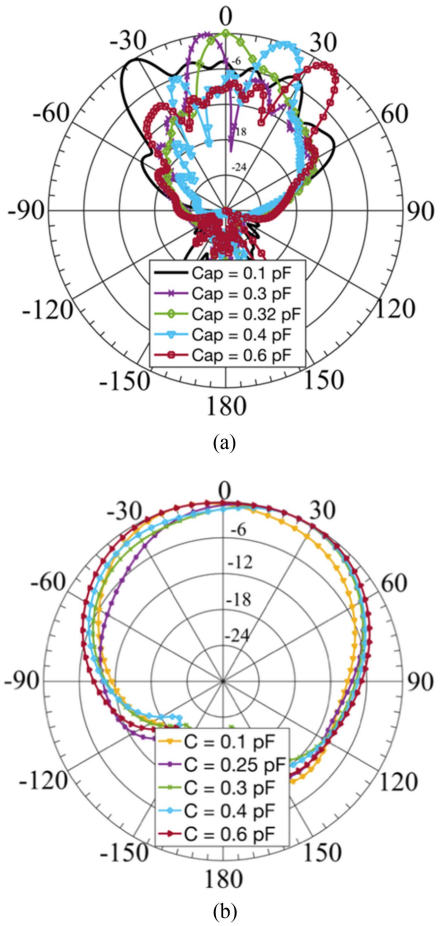

FIGURE 11. (a) Normalized radiation pattern in E-plane (xz-plane) (b) normalized radiation pattern in H-plane (yz-plane) with FPMS unit cells at 12 GHz.

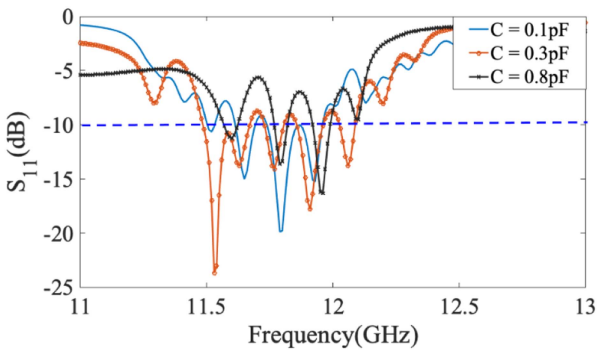

FIGURE 12. Reflection coefficient of LWA-2 with FPMS unit cells.

At the same time, the antenna's reflection coefficient (S_{11}) shows stable matching conditions at 12 GHz (∼11.95 GHz), Fig. 12. The results shown in this section illustrate that as the dielectric constant on the edge of the waveguide is modified, the antenna beam steers around the bore-sight direction. A key observation is that even with an effective negative permittivity

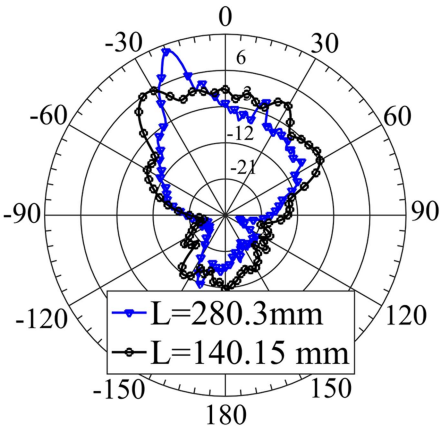

FIGURE 13. Radiation pattern of LWA in E-plane with different lengths.

due to the FPMS unit cells, acceptable gain performance is obtained. When the FPMS unit cells exhibit positive permittivity to the incoming wave, the structure behaves like a nominal waveguide with the conventional boundary conditions. On the other hand, with the negative permittivity at one of the edges of the waveguide, the wave is still trapped within the guided structure and the propagation is still possible but with modified boundary conditions on the FPMS edge. Thus, the antenna radiates well in both the states albeit with varying direction of radiation due to the change in the phase and propagation constant of the wave.

It can be appreciated that the impedance matching of such a reconfigurable design is quite a challenge. To make sure that the antenna is well-matched for all the bias conditions requires a decent optimization of the input feed structure. This process is carried out with the help of the tapered microstrip feed line. A series of simulations are performed in the software to make sure that the parameters of the antenna feed provide at least −10 dB of reflection coefficient for all varactor bias conditions, shown in Fig. 12. As minimum condition of −10 dB reflection coefficient is met for all capacitance values, the design can be taken forward for an actual validation through a fabricated prototype. Another important aspect that cannot be overlooked here is the modest gain of the antenna. LWAs are usually known to provide high gain and radiation efficiencies. For this design, a much better gain with an improved efficiency can be achieved by increasing the length of the structure. However, this requires an added number of FPMS unit cells or in other words varactors. For instance, if the antenna length is doubled with 149 varactor diodes, the gain can be increased to ∼13 dBi with an efficiency of $> 75\%$. But each varactor diode brings with it an added DC block capacitor and an RF choke resistor resulting in significantly increased complexity. Therefore, it would be wise to realize a less complex design with modest radiation performance and validate the proof-of-concept beam steering rather than choosing the best performing antenna.

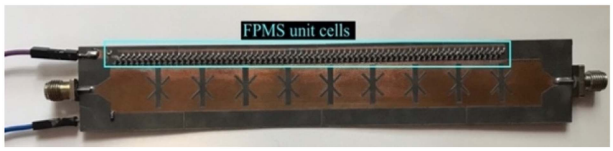

FIGURE 14. Fabricated prototype of LWA.

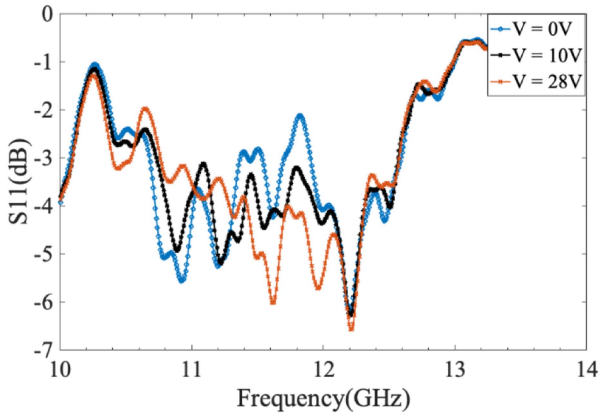

(a)

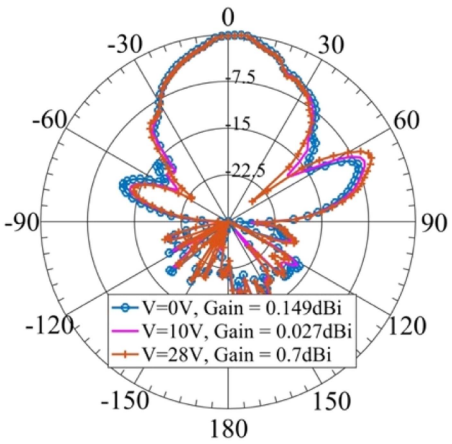

(b)

FIGURE 15. (a) S_{11} of LWA with integrated varactor diode at 12 GHz (b) measured radiation pattern.

V. LWA PROTYTPE WITH VARACTOR DIODES

A pictorial depiction of the fabricated LWA design with integrated varactor diodes is shown in Fig. 14. As in simulations, a total of 70 diodes are used in this structure for proper biasing of the FPMS unit cells. For simplicity, the diodes are biased using a single DC source resulting in the same applied voltage on all the unit cells. This kind of configuration limits the characterization scenarios for this antenna; however, at this stage, the simplification of testing is given preference over multiple measurement scenarios. Three values of DC bias, 0V, 10V, and 28 V, are used to plot the measured reflection coefficient of the antenna in Fig. 15(a). These values correspond to 1 pF, 0.45 pF, and 0.3 pF capacitances, respectively. A close observation of these measurements shows that the antenna does not have a

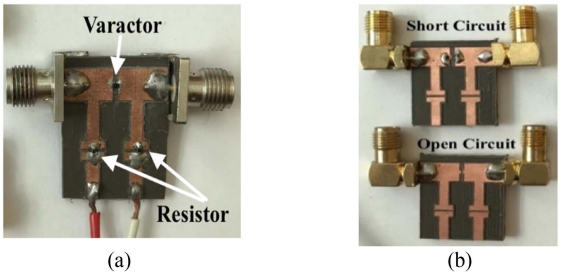

FIGURE 16 (a). Varactor PCB (b) open-short de-embedding structure.

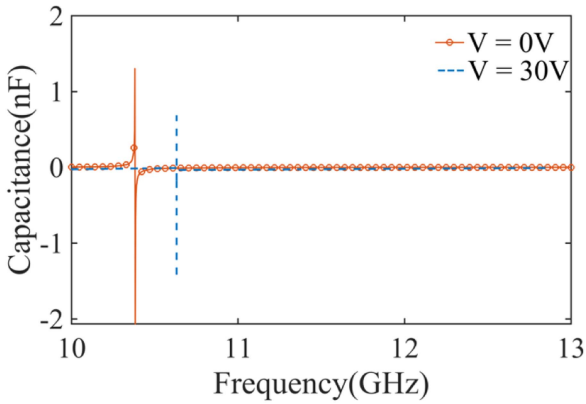

FIGURE 17. Self-resonance frequency of varactor at 0 V and 30 V.

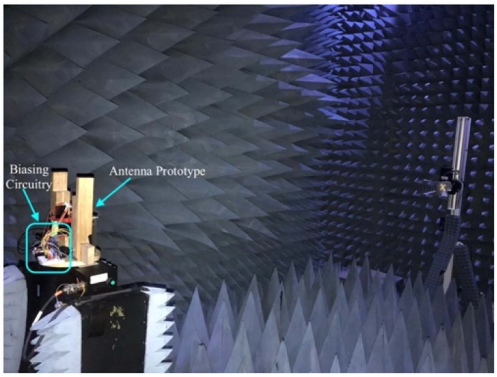

FIGURE 18. LWA measurement in an anechoic chamber.

good matching condition in any of the three cases at 12 GHz. However, this effect could be due to poor impedance matching at the input, and therefore to ascertain the complete antenna performance, it is important to characterize it for its radiation performance. The measured radiation patterns for the above-stated bias conditions are shown in Fig. 15(b). Unlike the simulation results, the beam steering is completely absent in the measured results. The maximum gain value is observed to be 0.7 dBi as opposed to the simulated value of 6.4 dBi at 0.3 pF capacitance. The two results i.e., impedance and radiation performance of the antenna in tandem, show considerable inconsistency between the simulated and measured data. To understand why the fabricated prototype is unable to confirm the simulation scenario, a closer look at the antenna prototype is needed to troubleshoot the problem.

VI. ANALYSIS OF VARACTOR BASED LWA DESIGN

In order to identify the exact reasons for the measurement results' discrepancies with the simulated ones, the varactor diode is first studied to validate its performance at 12 GHz. To carry out this study, a simple prototype with the appropriate bias circuitry is fabricated and shown in Fig. 16(a). By measuring the S-parameters of the varactor diode, one can extract the lumped component values vs. its bias at 12 GHz. The effect of the input and output interconnect transmission lines is de-embedded using short and open standards, as shown in Fig. 16(b). This step is helpful to eradicate any extra inductance added onto the measured data of the varactor by the interconnects. Using the imaginary part of the measured impedance, the capacitance of the varactor is extracted and plotted in Fig. 17 for the two extreme bias conditions i.e 0 V and 30 V. Interestingly, it is observed that the SRF (self-resonating frequency) of the diode is well below 12 GHz (around 10.5 GHz). This implies that the diode is working as a lossy inductor rather than as a capacitor at the frequency of interest. This explains the reason for poor radiation performance of the antenna. Since the diode is unable to provide the right capacitance values, the phase constant along the LWA structure is not the same as in simulations hence the malfunctioning of the proposed LWA.

These results provide a stimulating insight into the varactor-loaded LWA. Having completed these measurements, finding a different technique to validate the antenna performance of the design shown in Fig. 1 in a practical sense is imperative. Therefore, the authors proceeded to measure the antenna with fixed capacitors in place of varactor diodes to get some initial results of beam steering.

VII. ANTENNA MEASURMENT WITH FIXED CAPACITORS

As an alternate to the varactor diodes, surface-mount lumped capacitors of 0.1 pF and 0.3 pF are used to study the antenna radiation and impedance performance. Due to the absence of the bias structure, a simpler layout of the antenna is designed and fabricated for this run. This eliminates extra variables at this stage and allows for further troubleshooting of the proposed design. The prototype antennas are measured in an anechoic chamber to characterize their gain and radiation performance. A pictorial representation of the measurement setup can be seen in Fig. 18.

In the first case (0.1 pF), the maximum peak gain of the antenna is 4.2 dBi at −35°, which is comparable to the simulated value as shown in Fig. 19. Using the xz plane and 12 GHz as the center frequency, these results are compared herewith. Likewise, for the case of 0.3 pF, the simulated and measured radiation patterns are shown in Fig. 20. The antenna radiates with its maximum at 0° and a gain of 6.2 dBi that has a sound correlation with the simulated value of 6.4 dBi at −5°. These

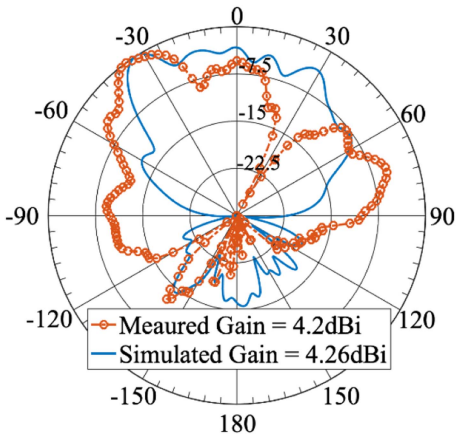

FIGURE 19. Simulated and measured co-polarized radiation pattern at 12 GHz with 0.1 pF.

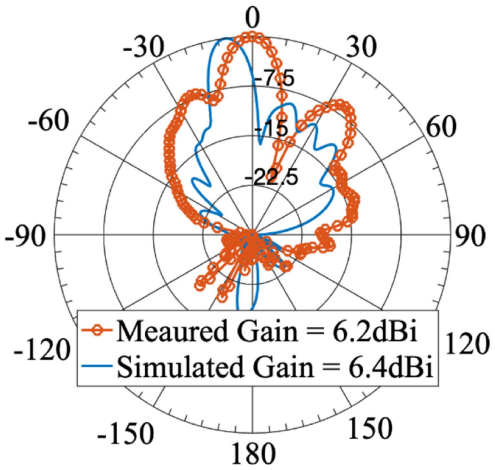

FIGURE 20. Simulated and measured co-polarized radiation pattern at 12 GHz (A) with 0.1 pF (B) 0.3 pF.

results demonstrate a measured beam steering of 35° that is not too different from the simulated value of 30°. The radiation pattern results of the fixed capacitor antenna prototype validate the realization of beam steering from FPMS unit cells which was not seen in the earlier prototype.

Afterwards, the two prototypes are also measured for their impedance performance to verify the matching conditions seen by the incoming wave. Both these cases show minimum reflection of the wave. This is validated by the curve of Fig. 21 for the case of 0.3 pF capacitance. To avoid redundancy, only one of the cases is presented here. These impedance results back the radiation performance of the antenna discussed in this section. Better matching performance can be seen in the simple capacitor-loaded antenna than the varactor based one. This is quite expected as it is relatively convenient to optimally match the LWA design with a single capacitor value. Rest assured, the antenna prototypes show good impedance and radiation performance to validate the proof-of-concept of

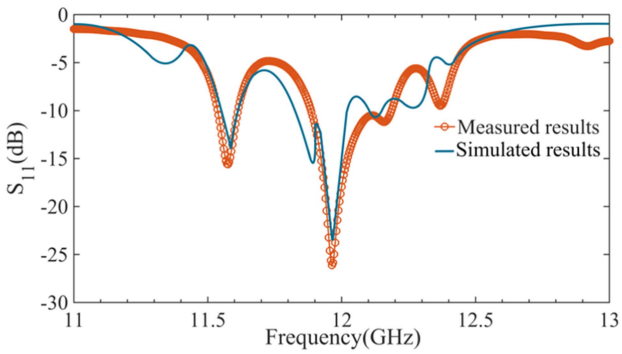

FIGURE 21. Simulated and measured S_{11} of LWA with 0.3 pF.

an FPMS integrated LWA antenna. Although the final prototype is not able to provide maximum steering of 72°, the authors believe that this limitation is due to the varactor and capacitor values selection and not because of the antenna design concept. With the right selection of the component values the maximum value of antenna steering can be realized in a fabricated prototype.

VIII. COMPARISON WITH THE STATE OF THE ART

A comparison of the state-of-the-art literature with the antenna presented in this article is tabulated in this section (Table 2) for the benefit of the readers. If one limits the focus on the X-band, it can be easily deduced that not many examples of LWA design exist in literature for single frequency operation. The results of steering provided in [25], [26] are quite intriguing; however, the antenna fabrication is quite complex in both these examples. Similarly, the reconfigurability achieved in [27], [28], [29] is quite wide over the plane, however, the designs are unable to provide continuous steering as is shown. The use of varactors is also demonstrated in [30], [31], [32] with efficient gain performance and continuous steering. However, the range in these designs is limited. The popularity of microstrip based LWA designs is evident from the series of antennas reported in the last few years [33], [34], [35], [36], [37]. Among these, a dual-band antenna is reported with decent steering performance, however, the design is unable to overcome the open stop band region [35]. The drawback of the antenna reported in [36] is its poor matching performance while the antenna of [37] can only steer the beam in a range of ±25° degrees and that too only discretely. The distinguishing factor of [38] is the use of slotted horn antenna to demonstrate an LWA structure. As is expected, the antenna gain is high showing efficient radiation performance, however the beam scanning is limited to forward quadrant only. The most recent publication among these is based on a grove gap waveguide structure with the best gain in Table 2 [39]. However, when the antenna steers to the broadside direction, it radiates inefficiently. To summarize, there are some antennas that provide single frequency beam steering using LWA concept but the concept of FPMS provides a whole new dimension to this class of antennas. The control provided

TABLE 2 Comparison of State-of-the-Art LWA Designs

Paper	Type of LWA	Max gain (dBi)	Frequency (GHz)	Active Components	Resolution steps	Beam steering range θ	Structure Complexity
[24]	Patch array	13.54	3.6	PIN diodes	Discrete step steering (10°)	94°	2 layers
[25]	Microstrip LWA	8.9	10	Varactor diodes	Continuous	130°	1 layer
[26]	Microstrip LWA	6-8	8	Varactor diodes	Continuous	118°	3 layers
[27]	SIW	11.8	5	PIN diodes	Discrete step steering (15°)	125°	4 layers
[28]	Metamaterial	11.12	5	PIN diodes	Discrete step steering (12°)	60°	3 layers
[29]	Microstrip LWA	10.34	7.5	Capacitive loading	Discrete step steering (20°)	160°	1 layer
[30]	HMSIW	9.5	6.5	Inter digital capacitors	Continuous	66°	1 layer
[31]	Fabory-Perot Leaky-waveguide	12.95	5.6	Varactor diodes	Continuous	21°	2 layers
[32]	Fabory-Perot Leaky-waveguide	13	5.5	Varactor diodes	Continuous	50°	2 layers
[33]	Microstrip LWA	12.9	6	PIN diodes	Discrete step steering (N/A)	29°	1 layer
[34]	Microstrip LWA	10	9.8	PIN diodes	Discrete step steering (5°)	15°	1 layer
[35]	Microstrip LWA	N/A	4.25 and 5.75	Varactor diodes	Continuous	80°	1 layer
[36]	Microstrip LWA	8.2	4.75-5.25	-	Continuous	100°	2 layers
[37]	Microstrip LWA	7.7	2.45	PIN diodes	Discrete step steering (N/A)	50°	1 layer
[38]	Horn Antenna	11.8	9.3	Varactors	Continuous	43°	1 layer
[39]	Groove gap waveguide LWA	16.8	27 and 28	PIN diodes	Discrete step steering (~10°)	110°	3 layers
This work	**HMSIW**	**6.2**	**12**	**FPMS unit cells**	**Continuous**	**72°**	**1 layer**

by FPMS is quite unique that modulates the substrate properties to achieve the desired results. Furthermore, the use of FPMS technology is not limited to LWA designs and can be extended to other class of antennas for demonstration of new and intelligent radiating elements that illustrates the benefits of this technology.

IX. CONCLUSION

This work validates the use of FPMS technology for the design of smart antenna systems and provides a basis for reconfigurable antenna designs using this new technology. With the help of fixed capacitors, acceptable beam steering is obtained from the proposed antenna structure. The design provides a measured steering range of 35° at 12 GHz. With a working varactor diode, this range can be further enhanced to achieve better beam steering results. If a varactor with a high SRF is used with this design, such as MACOM's MA46580-1209, then significantly better impedance and radiation performance can be attained. It is believed that the simulated beam steering of 72° can be materialized. Using this work as a proof-of-concept, providing some preliminary results, FPMS technology can be further enhanced for its employability in design of smart antenna systems for various RF applications.

REFERENCES

[1] A. A. Oliner, "Leaky-wave antennas," in *Antenna Engineering Handbook*, R. C. Johnson, Ed., 3rd ed. New York, NY, USA: McGraw-Hill, 1993, p. 10-3, ch. 10.

[2] J. du Preez and S. Sinha, "Leaky-wave antennas," in *Millimeter-Wave Antennas: Configurations and Applications*, Berlin, Germany: Springer, 2016, pp. 19–38.

[3] P. Hudec, P. Panek, and V. Jenik, "Multimode adaptable microwave radar sensor based on leaky-wave antennas," *IEEE Trans. Microw. Theory Techn.*, vol. 65, no. 9, pp. 3464–3473, Sep. 2017.

[4] A. K. Tiwari, S. Awasthi, and R. K. Singh, "A symmetrical periodic leaky-wave antenna with backward-to-forward scanning," *IEEE Antennas Wireless Propag. Lett.*, vol. 19, no. 4, pp. 646–650, Apr. 2020.
[5] A. Sarkar, A. Sharma, A. Biswas, and M. J. Akhtar, "EMSIW-based compact high gain wide full space scanning LWA with improved broadside radiation profile," *IEEE Trans. Antennas Propag.*, vol. 67, no. 8, pp. 5652–5657, Aug. 2019.
[6] S. K. Podilchak, A. P. Freundorfer, and Y. M. M. Antar, "Surface-wave launchers for beam steering and application to planar leaky-wave antennas," *IEEE Trans. Antennas Propag.*, vol. 57, no. 2, pp. 355–363, Feb. 2009.
[7] P. Lu et al., "InP-based THz beam steering leaky-wave antenna," *IEEE Trans. THz Sci. Technol.*, vol. 11, no. 2, pp. 218–230, Mar. 2021.
[8] K. Murano et al., "Low-profile terahertz radar based on broadband leaky-wave beam steering," *IEEE Trans. THz Sci. Technol.*, vol. 7, no. 1, pp. 60–69, Jan. 2017.
[9] J. Liu and Y. Long, "Analysis of a microstrip leaky-wave antenna loaded with shorted stubs," *IEEE Antennas Wireless Propag. Lett.*, vol. 7, pp. 501–504, 2008.
[10] J. Liu, D. R. Jackson, Y. Li, C. Zhang, and Y. Long, "Investigations of SIW leaky-wave antenna for endfire- radiation with narrow beam and sidelobe suppression," *IEEE Trans. Antennas Propag.*, vol. 62, no. 9, pp. 4489–4497, Sep. 2014.
[11] Y. Geng, J. Wang, Y. Li, Z. Li, M. Chen, and Z. Zhang, "Radiation pattern-reconfigurable leaky-wave antenna for fixed-frequency beam steering based on substrate-integrated waveguide," *IEEE Antennas Wireless Propag. Lett.*, vol. 18, no. 2, pp. 387–391, Feb. 2019.
[12] M. K. Mohsen, M. S. M. Isa, A. A. M. Isa, M. K. Abdulhameed, and M. L. Attiah, "Achieving fixed-frequency beam scanning with a microstrip leaky-wave antenna using double-gap capacitor technique," *IEEE Antennas Wireless Propag. Lett.*, vol. 18, no. 7, pp. 1502–1506, Jul. 2019.
[13] M. Wang, H. F. Ma, H. C. Zhang, W. X. Tang, X. R. Zhang, and T. J. Cui, "Frequency-fixed beam-scanning leaky-wave antenna using electronically controllable corrugated microstrip line," *IEEE Trans. Antennas Propag.*, vol. 66, no. 9, pp. 4449–4457, Sep. 2018.
[14] A. Sarkar, A. Sharma, A. Biswas, and M. J. Akhtar, "Compact CRLH leaky-wave antenna using TE20 mode substrate integrated waveguide for broad space radiation coverage," *IEEE Trans. Antennas Propag.*, vol. 68, no. 10, pp. 7202–7207, Oct. 2020.
[15] A. Sarkar et al., "Composite right/left-handed based compact and high gain leaky-wave antenna using complementary spiral resonator on HMSIW for Ku band applications," *IET Microw. Antennas Propag.*, vol. 12, no. 8, pp. 1310–1315, 2018.
[16] N. Jess, B. A. Syrett, and L. Roy, "The field-programmable microwave substrate," *IEEE Trans. Microw. Theory Techn.*, vol. 64, no. 11, pp. 3469–3482, Nov. 2016.
[17] H. Xu, Y. Wang, F. A. Ghaffar, and L. Roy, "Reconfigurable microwave filters implemented using field programmable microwave substrate," *IEEE Trans. Microw. Theory Techn.*, vol. 69, no. 2, pp. 1344–1354, Feb. 2021.
[18] S. Ali, F. A. Ghaffar, and H. M. Cheema, "Beam steerable leaky wave antenna using FPMS," in *Proc. IEEE Int. Symp. Antennas Propag. USNC-URSI Radio Sci. Meeting*, 2021, pp. 1005–1006.
[19] N. K. Roy and F. A. Ghaffar, "A novel microstrip line based leaky wave antenna using capacitive loading," in *Proc. IEEE 19th Int. Symp. Antenna Technol. Appl. Electromagn.*, 2021, pp. 1–2.
[20] D. René-Loxq, O. Lafond, M. Himdi, L. Roy, and F. Ghaffar, "Reconfigurable half-mode SIW antenna using uniaxial field programmable microwave substrate structure," *IEEE Trans. Antennas Propag.*, vol. 70, no. 11, pp. 11103–11108, Nov. 2022.
[21] L. F. Chen, C. K. Ong, C. P. Neo, V. V. Varadan, and V. K. Varadan, *Microwave Electronics: Measurement and Materials Characterization*. Hoboken, NJ, USA: Wiley, 2004.
[22] N. Javanbakht, M. S. Majedi, and A. R. Attari, "Thinned array inspired quasi-uniform leaky-wave antenna with low side-lobe level," *IEEE Antennas Wireless Propag. Lett.*, vol. 16, pp. 2992–2995, 2017.
[23] K. D. Karmokar and Y. J. Guo, "Continuous backward- to- forward beam-scanning conformal leaky-wave antenna," in *Proc. IEEE Asia-Pacific Conf. Antennas Propag.*, 2018, pp. 72–73.
[24] X. Cao, C. Deng, and K. Sarabandi, "Fixed-frequency beam steering leaky-wave antenna with integrated 2-bit phase shifters," *IEEE Trans. Antennas Propag.*, vol. 70, no. 11, pp. 11246–11251, Nov. 2022.
[25] G. Xu, G. V. Eleftheriades, and S. V. Hum, "Wide-angle beam-steering and adaptive impedance matching with reconfigurable non-local leaky-wave antenna," *IEEE Open J. Antennas Propag.*, vol. 3, pp. 1141–1153, 2022.
[26] H.-H. Lv, Q.-L. Huang, J.-Q. Hou, and X.-W. Shi, "Fixed-frequency beam-steering leaky-wave antenna with switchable beam number," *IEEE Antennas Wireless Propag. Lett.*, vol. 19, no. 12, pp. 2077–2081, Dec. 2020, doi: 10.1109/LAWP.2020.302281.
[27] Z. Li, Y. J. Guo, S.-L. Chen, and J. Wang, "A period-reconfigurable leaky-wave antenna with fixed-frequency and wide-angle beam scanning," *IEEE Trans. Antennas Propag.*, vol. 67, no. 6, pp. 3720–3732, Jun. 2019, doi: 10.1109/TAP.2019.29.
[28] Y. Luo, K. Qin, H. Ke, B. Xu, S. Xu, and G. Yang, "Active metamaterial antenna with beam scanning manipulation based on a digitally modulated array factor method," *IEEE Trans. Antennas Propag.*, vol. 69, no. 2, pp. 1198–1203, Feb. 2021.
[29] R. O. Ouedraogo, E. J. Rothwell, and B. J. Greetis, "A reconfigurable microstrip leaky-wave antenna with a broadly steerable beam," *IEEE Trans. Antennas Propag.*, vol. 59, no. 8, pp. 3080–3083, Aug. 2011.
[30] A. Suntives and S. V. Hum, "A fixed-frequency beam-steerable half-mode substrate integrated waveguide leaky-wave antenna," *IEEE Trans. Antennas Propag.*, vol. 60, no. 5, pp. 2540–2544, May 2012.
[31] R. Guzman-Quiros, J. L. Gomez-Tornero, A. R. Weily, and Y. J. Guo, "Electronically steerable 1-D Fabry-Perot leaky-wave antenna employing a tunable high impedance surface," *IEEE Trans. Antennas Propag.*, vol. 60, no. 11, pp. 5046–5055, Nov. 2012.
[32] R. Guzman-Quiros, J. L. Gomez-Tornero, A. R. Weily, and Y. J. Guo, "Electronic full-space scanning with 1-D Fabry–Pérot LWA using electromagnetic band-gap," *IEEE Antennas Wireless Propag. Lett.*, vol. 11, pp. 1426–1429, 2012.
[33] D. K. Karmokar, K. P. Esselle, and S. G. Hay, "Fixed-frequency beam steering of microstrip leaky-wave antennas using binary switches," *IEEE Trans. Antennas Propag.*, vol. 64, no. 6, pp. 2146–2154, Jun. 2016.
[34] X. Wan, T. Y. Chen, X. Q. Chen, L. Zhang, and T. J. Cui, "Beam forming of leaky waves at fixed frequency using binary programmable metasurface," *IEEE Trans. Antennas Propag.*, vol. 66, no. 9, pp. 4942–4947, Sep. 2018.
[35] M. Wang, H. F. Ma, W. X. Tang, H. C. Zhang, W. X. Jiang, and T. J. Cui, "A dual-band electronic-scanning leaky-wave antenna based on a corrugated microstrip line," *IEEE Trans. Antennas Propag.*, vol. 67, no. 5, pp. 3433–3438, May 2019.
[36] L. Chen, D. K. Karmokar, Z. Li, P.-Y. Qin, R. W. Ziolkowski, and Y. J. Guo, "Continuous beam scanning at a fixed frequency with a composite right-/left-handed leaky-wave antenna operating over a wide frequency band," *IEEE Trans. Antennas Propag.*, vol. 67, no. 12, pp. 7272–7284, Dec. 2019.
[37] R. Shaw and M. K. Mandal, "Broadside scanning fixed frequency LWA with simultaneous electronic control of beam angle and beamwidth," *IEEE Trans. Antennas Propag.*, vol. 68, no. 5, pp. 3504–3514, May 2020.
[38] A. Ohadi and G. V. Eleftheriades, "Fixed-frequency beam-steering using slotted waveguide with tunable impedance walls," *IEEE Open J. Antennas Propag.*, vol. 2, pp. 978–990, 2021.
[39] S. Liu, Z. Li, and J. Wang, "A fixed-frequency beam-scanning leaky-wave antenna using phase and amplitude control for millimeter-wave applications," *IEEE Trans. Antennas Propag.*, vol. 71, no. 2, pp. 1568–1577, Feb. 2023.

SHAHINSHAH ALI (Student Member, IEEE) received the B.E. degree in electronics engineering from the Ghulam Ishaq Khan Institute of Engineering Sciences and Technology, Topi, Pakistan, in 2017, and the M.S. degree in electrical engineering (RF and Microwave) from the National University of Sciences & Technology (NUST), Islamabad, Pakistan, in 2022. He is currently working toward the Ph.D. degree in electrical engineering with Lakehead University, Thunder Bay, ON, Canada. He was with the RADAR Lab, School of Interdisciplinary Engineering & Science, NUST, Islamabad, as an Antenna Design Engineer. His research interests include antenna designing, and RF and Microwave systems.

HAMMAD M. CHEEMA (Senior Member, IEEE) received the bachelor's degree in electrical engineering from the National University of Sciences & Technology (NUST), Islamabad, Pakistan, the M.Sc. degree in telecommunications from the Technical University of Denmark, Kongens Lyngby, Denmark, and the Ph.D. degree in electrical engineering from the Eindhoven University of Technology, Eindhoven, The Netherlands. His Ph.D. research was related to integrated circuit design of phase locked loops and millimeter wave components for 60 GHz broadband wireless transceivers. From 2011 to 2013, he was a Postdoctoral Researcher with the IMPACT Lab, KAUST, Saudi Arabia working on 60 GHz transmitter chips and on-chip antennas. He was also on flexible and printed electronics for low-cost inkjet printed applications using paper and plastic substrates. He is currently the Principal & Dean School of Interdisciplinary Engineering & Sciences, NUST, working on MMICs and radar front-ends. His industrial experience include various technical roles with Motorola & Ericsson in Pakistan, and Danske Telecom, Accenture and Microsoft in Denmark. He has authored more than 70 journal and conference papers, two books and twelve pending/awarded patents. He was the recipient of the Best University Teacher Award in 2015, Best Institute Researcher Award in 2019, and Best Institute Innovator Award in 2022.

FARHAN A. GHAFFAR (Senior Member, IEEE) received the B.E. degree in electronics engineering from the NED University of Engineering and Technology, Karachi, Pakistan, in 2007, and the M.S. and Ph.D. degrees in electrical engineering from the King Abdullah University of Science and Technology (KAUST), Thuwal, Saudi Arabia, in 2010 and 2016, respectively. Before joining Lakehead University, Thunder Bay, ON, Canada, as an Assistant Professor with the Department of Electrical Engineering, he was a Postdoctoral Fellow/Instructor with Ontario Tech University, Oshawa, ON, Canada, from January 2017 to July 2019. From 2008 to 2009, he was an Assistant Manager with Space and Upper Atmosphere Research Commission (SUPARCO) of Pakistan. He was invited as a Visiting Researcher with Carleton University and Royal Military College, in 2010 and 2012, respectively. He has authored or coauthored more than 35 international publications which include 20 peer-reviewed journal papers. He is a Co-Inventor on five international patents. His research interests include the design of system-on-package and system-on-a-chip-based antennas, radio frequency integrated circuits, flexible microwave passive components, and ferrite low temperature co-fired ceramic-based tunable antennas and passives. He was the recipient of the Academic Excellence Award at KAUST in 2013 and 2015, secured Honorary Mention in the First Ever 3MT Competition at International Microwave Symposium (IMS), and Best Performance Award at SUPARCO in 2009.